SickKids
THE HOSPITAL FOR SICK CHILDREN

CIGITI Centre for Image Guided Innovation & Therapeutic Intervention

SIX-MONTH REPORT:

Project: Non-Invasive Treatment of Pediatric Neurological Disorders using MR-guided Focused Ultrasound (MRgFUS) – Part 1 Pediatric Skull Characterization and Re-Focusing

1. Introduction:

Pediatric neurological diseases such as stroke and epilepsy are disproportionally common: stroke is highest in the perinatal period and occurs in 1 in 3000 live births. Epilepsy affects 1% of all children and up to 30% of these will develop drug resistant seizures leading to a lifetime of medical disability. Neonatal and pediatric skulls have unique anatomical characteristics such as an open fontanelle, a thinner skull and reduced acoustic attenuation. The project hypothesizes that these characteristics make them ideal candidates for MRgFUS treatment, since their natural features simplifies the challenge of transcranial sonication and reduces the need for large hemispherical transducers.
As there is minimal literature on the subject, the first part of the project is to perform the acoustic characterization of pediatric skulls ranging from 0 to 16 years old. Then the aim is to study the acoustic propagation near these skulls and develop an algorithm for re-focusing across these skulls. In this report we present our current results regarding insertion losses (IL) and time of flight (TOF) delay with two skull specimens. Ultimately, these two types of measurements are the experimental input data that will be used to calculate the speed of sound and attenuation coefficient of the skull for neonatal and young humans.

2. Pediatric skull library:

Two cadaveric pediatric skulls have been obtained: A neonate skull with an open fontanelle and an 8-year old skull (Figure 1). A phantom skull, made from a bone-mimicking ceramic, representing the 8-year old skull has also been manufactured by the group of Dr. Roman Maev from the University of Windsor *(Wydra et al., 2013)*.

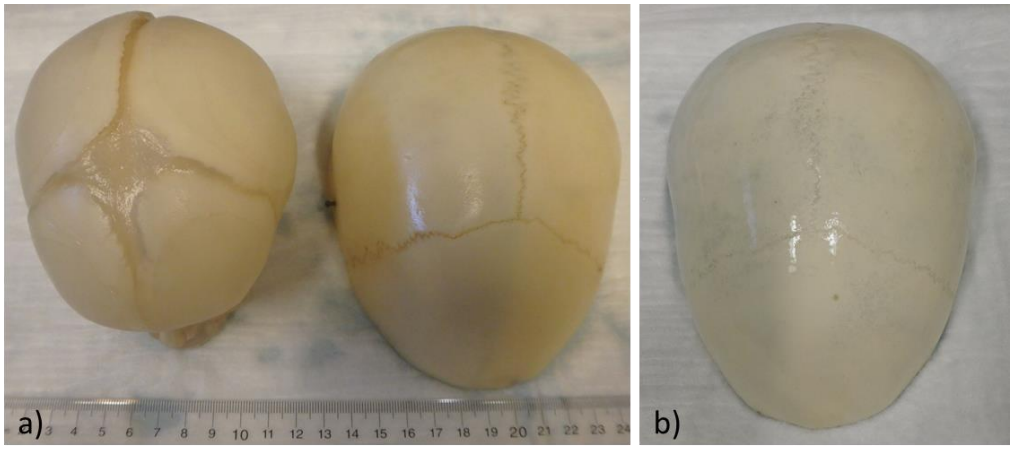

Figure 1: Pediatric skull library: a) on the left the neonate skull, on the right the 8-year old skull, b) the phantom skull

3. Pediatric skull characterization methods:

The skull is first degassed for 48h at -29 "Hg before starting to work with it and then degassed again for 12h before each experiment. A 0.2 mm needle acoustic hydrophone is then placed in a tank of degassed water and aligned to the geometric focus of a clinical HIFU transducer (Philips Sonalleve V1). The signals of the 256 elements of the phased array transducer are acquired as a baseline measurement using this hydrophone and the MatHIFU software toolkit *(Zaporzan et al., 2013)*. The degassed skull is placed inside the tank between the hydrophone and the transducer. New acquisitions are performed for different angular orientations of the skull according to the sagittal and coronal axes in the range of ± 15° (Figure 2). Insertion losses (IL) and time-of-flight (TOF) delays due to the skull and the fontanelle, if present, are deducted from these measurements performed at 1 MHz, 1.2 MHz and 1.45 MHz. Time-of-flight (TOF) delay due to the skull is obtained by calculating the difference between the skull and baseline TOF measurements for each orientation and each frequency. The Insertion Loss (IL) is obtained by calculating the difference between the root mean square (RMS) amplitude of the skull signals and the baseline RMS amplitude for each orientation and each frequency.

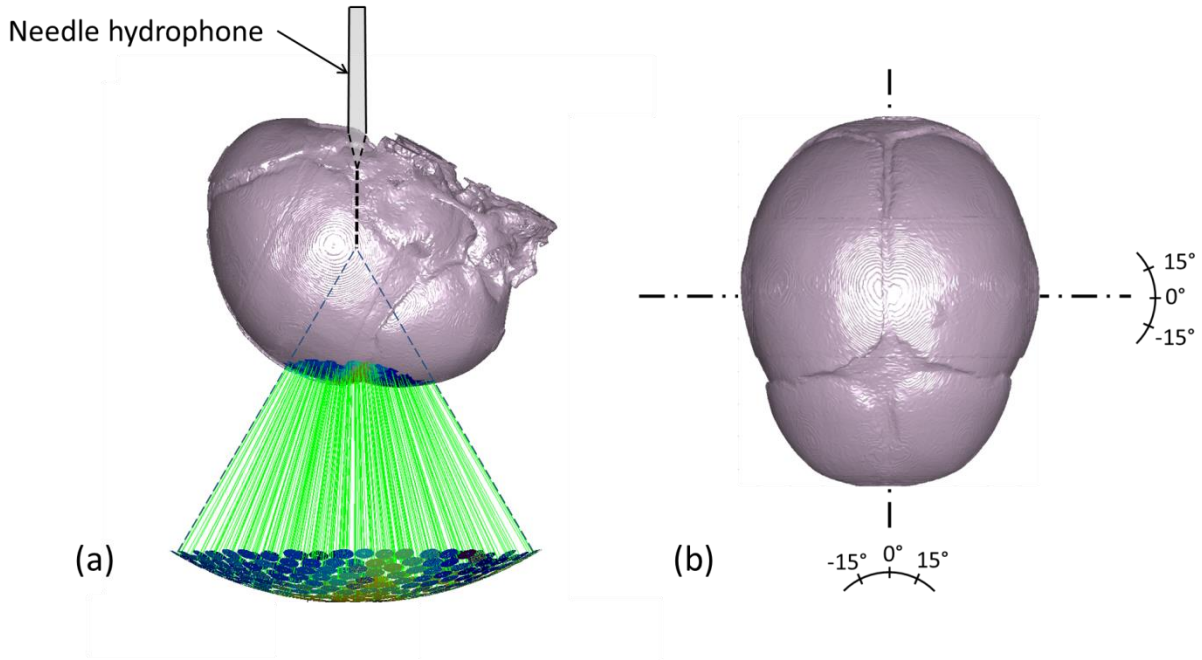

Figure 2: (a) Illustration of the experimental set up showing the skull positioning at 0° between the hydrophone and the transducer. The green lines represent the beam paths crossing the skull surface; (b) Illustration of the different angular orientations of the skull.

4. Acoustic properties of the neonate skull:

TOF delay and IL due to the neonate skull were measured at 1, 1.2 and 1.45 MHz. MRI acquisitions of the skull and the transducer positioning were performed for each skull orientation using a large dual-channel flex coil in a Philips Achieva 3.0T TX scanner. A 200 µm-resolution segmented CT skull was then rigidly registered to the MRI skull to obtain a better resolution. TOF delay and IL values obtained for each transducer element were then projected on the CT skull surface. Parietal and frontal bones and fontanelle acoustic properties were then calculated.

a. Time-of-flight (TOF) delay results:

The fontanelle can be easily discriminated from the bone areas as it's TOF delay is very low (TOF $delay_{fontanelle}$ = -0.08 ± 0.02 µs over the frequency range) (Figure 3).
The TOF delay is constant over the frequency range and is globally the same for all bone areas (TOF $delay_{frontal}$ = -0.16 ± 0.02 µs and TOF $delay_{parietal}$ = -0.15 ± 0.02 µs) (Figure 4).

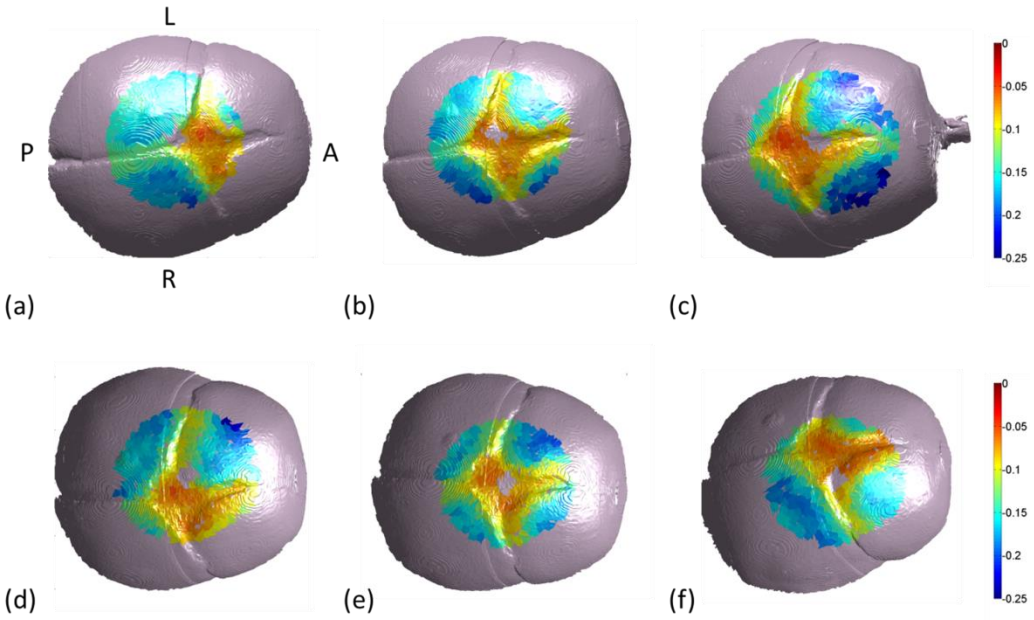

Figure 3: Projections of the TOF delays (µs) on the skull surface at 1.2 MHz for the different orientations: (a) 15° coronal showing the parietal bones, (b) 0° coronal showing the fontanelle, (c) -15° coronal showing the frontal bones, (d) 15° sagittal showing the left side of the skull, (e) 0° sagittal showing the fontanelle, (f) -15° sagittal showing the right side of the skull.

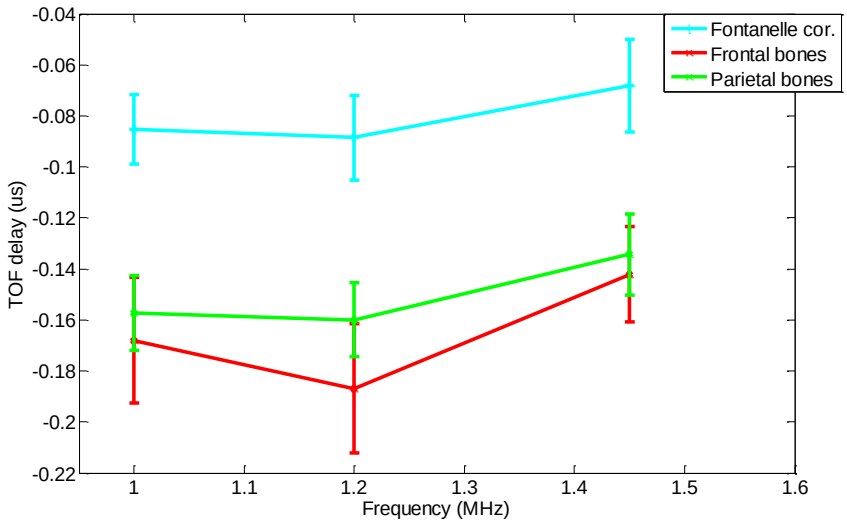

Figure 4: Evolution of the TOF delay (µs) with the frequency (MHz) for the different areas of interest. The average value and its standard deviation are represented for each area.

b. Insertion Loss (IL) results:

Higher dispersion of the IL values compared to the TOF delay values is observed (Figure 5). This is something expected as the IL depends on the incidence angle between the acoustic source and the skull bone. The fontanelle is still well demarcated as the IL in this area is very low ($IL_{fontanelle}$ = 0.8 ± 0.9 dB over the frequency range).

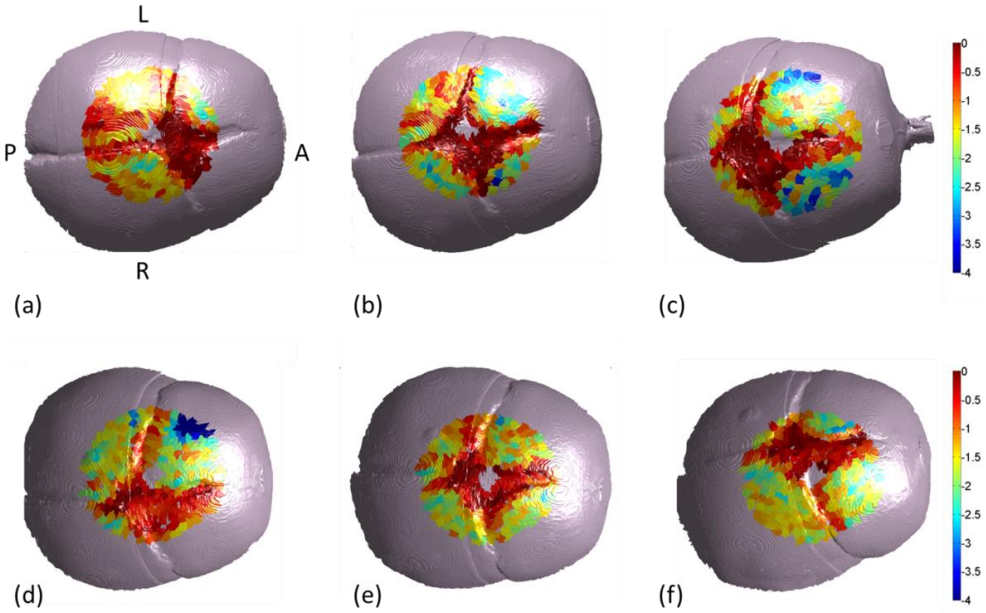

Figure 5: Projections of the IL (dB) on the skull surface at 1.2 MHz for the different orientations: (a) 15° coronal showing the parietal bones, (b) 0° coronal showing the fontanelle, (c) -15° coronal showing the frontal bones, (d) 15° sagittal showing the left side of the skull, (e) 0° sagittal showing the fontanelle, (f) -15° sagittal showing the right side of the skull.

Frontal bones lead globally to higher IL than parietal bones ($Il_{frontal}$ = 2.7 ± 1 dB against $Il_{parietal}$ = 1.9 ± 0.7 dB over the frequency range). The maximum IL value found is 3 ± 1 dB at 1 MHz and 1.45 MHz in the frontal bones (Figure 6). The IL decreases at 1.2 MHz for the frontal and parietal bones. This tendency is confirmed by looking at the values of some random points in these areas.

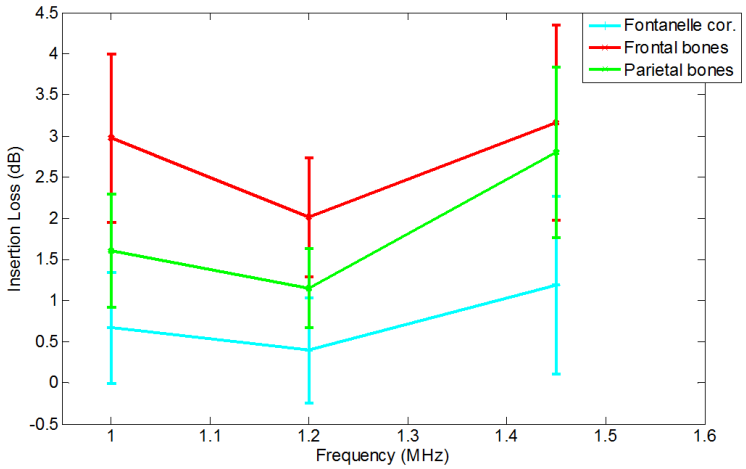

Figure 6: Evolution of the IL (dB) with the frequency (MHz) for different areas of interest. The average value and its standard deviation are represented for each area.

c. Discussion:

Aberration and attenuation effects due to the fontanelle are very low ($IL_{fontanelle}$ = 0.8 ± 0.9 dB and TOF $delay_{fontanelle}$ = -0.08 ± 0.02 µs over the frequency range). IL and TOF delays values of the neonate skull are low compared to adult skull values found in the literature (25 dB at 1MHz <$Il_{adult\ skull}$ < 42 dB at 1.45 MHz *(Fry et al., 1978)* and TOF $delay_{adult\ skull}$ ≈ -1.7µs at 1.4 MHz *(Pichardo et al., 2011)*). The neonate skull constitutes a weak acoustic barrier and its fontanelle can even act as an acoustic window.

5. Acoustic characterization of the 8-year old skull:

Acoustic characterization of the 8-year old skull is still ongoing. TOF delay and IL have been obtained at 1.2 MHz. The sagittal suture, the left and the right parietal bones have been studied.

a. TOF delay results:

At 1.2 MHz, the TOF delay for the sagittal suture, was -0.78 ± 0.22 µs. For the right and the left parietal bones, the TOF delays were -0.79 ± 0.11 and -0.71 ± 0.06 µs respectively. If the TOF delay is homogeneous in the bone areas, high dispersion of the TOF delay values was noted in the sagittal suture area (Figure 7). This can be due to the internal structure of the suture and also to bubbles being trapped even after several days of degassing.

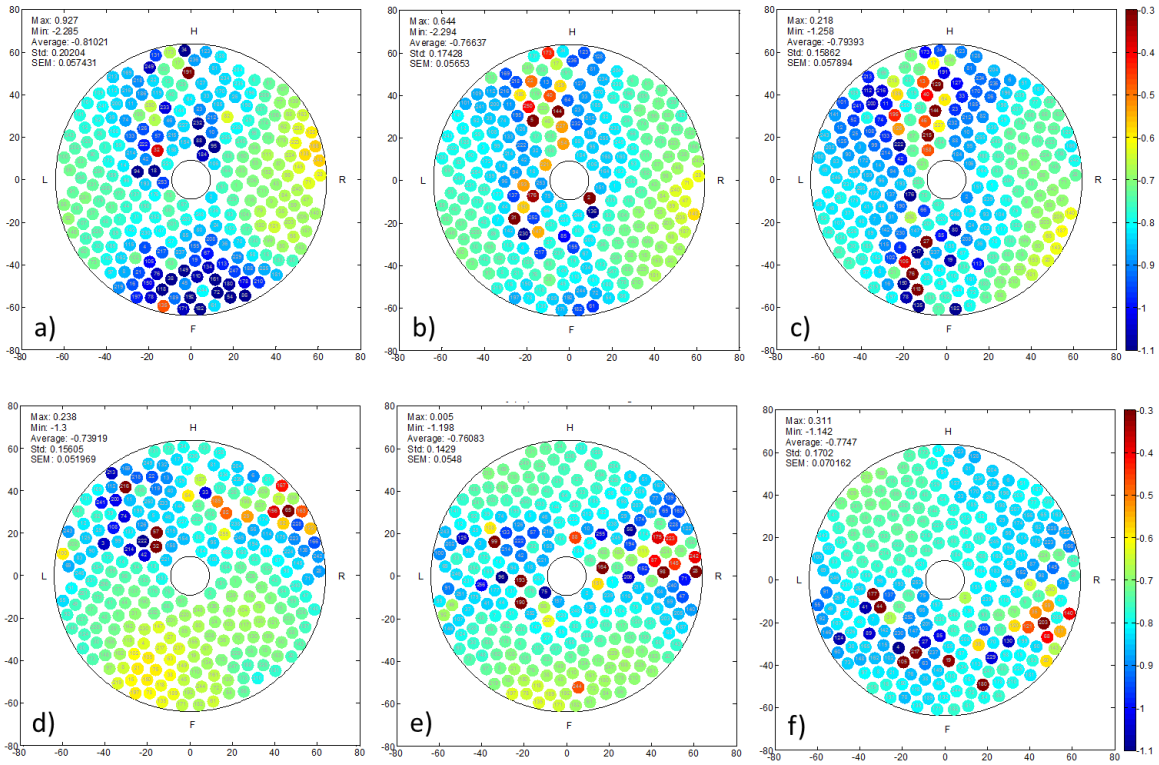

Figure 7: Average TOF delay values (us) obtained for each transducer element for each skull orientation. (a) -15° coronal, (b) 0° coronal centered on the sagittal suture, (c) 15° coronal, (d) -15° sagittal showing the values of the left side of the skull, (e) 0° sagittal centered on the sagittal suture, (f) 15° sagittal showing the values of the right side of the skull.

b. IL results:

At 1.2 MHz, for the sagittal suture, the IL was 14.2 ± 2.1 dB. For the right and the left parietal bones, the IL was 11.5 ± 1.6 and 8.3 ± 1.2 dB respectively. The difference between the sagittal suture and the parietal bones is much more visible when looking at the IL compared to the TOF delay. The sagittal suture leads to significant higher IL than the rest of the skull (Figure 8). This also can be due to the internal structure of the suture.

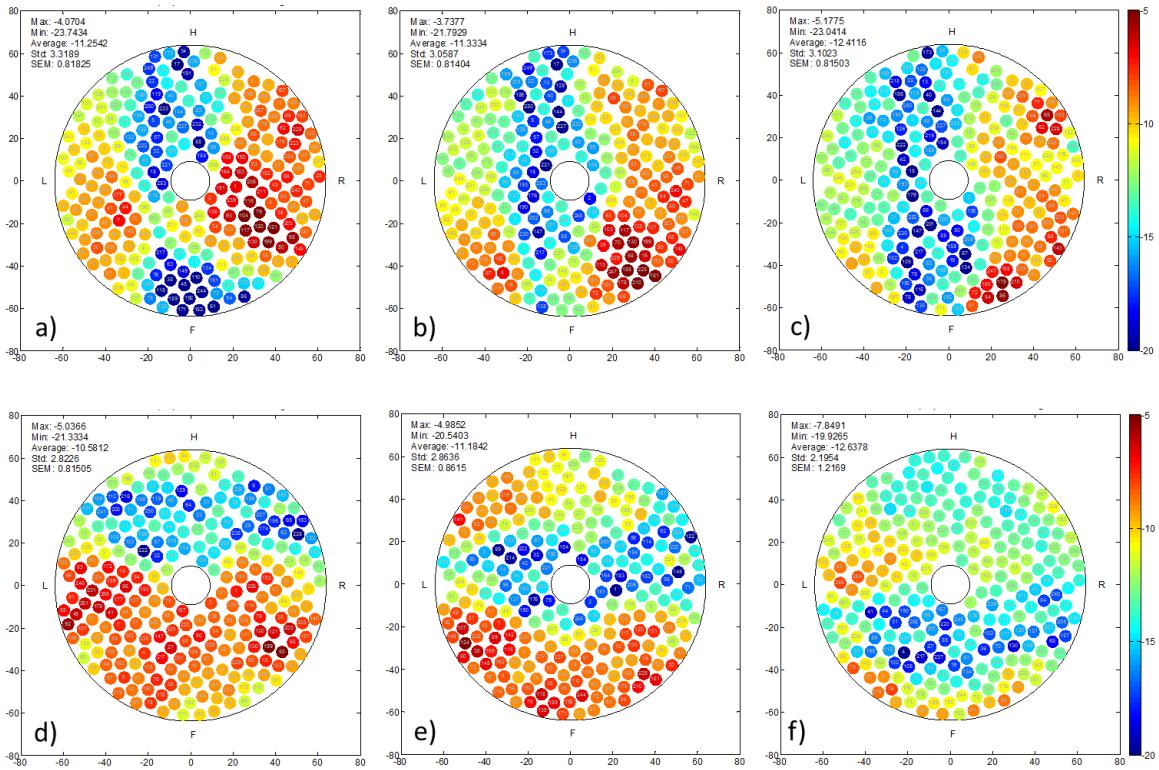

Figure 8: Average IL values (us) obtained for each transducer element for each skull orientation. (a) -15° coronal, (b) 0° coronal centered on the sagittal suture, (c) 15° coronal, (d) -15° sagittal showing the values of the left side of the skull, (e) 0° sagittal centered on the sagittal suture, (f) 15° sagittal showing the values of the right side of the skull.

c. Discussion:

As expected, the 8-y.o. skull bones have higher IL and TOF delays than the neonate ones but are still low compared to the adults ones found in the literature. The structure of the sagittal suture seems to have an impact on the propagation of ultrasound. This anatomical element will have to be taken into account in future numerical work.

6. Conclusions and future work:

Two cadaveric pediatric skulls have been obtained. One has been characterized and the other still under characterization. The results confirmed our hypothesis that ultrasound propagation seems easier through these skulls than through adult skulls. A phantom of the 8-year old skull has been manufactured and will be characterized using similar techniques. If it's results are close to the real one, other phantoms will be manufactured increasing our library of acoustic properties of the skull according to the

age of the patient from 2 to 16 years old, with one phantom per year of age. Speed of sound and attenuation in the neonate skull are under study based on our high resolution CT images and the orientation of the skull compared to the transducer elements. As mentioned previously, the IL and TOF delay is the basic experimental data that is required for ultimately calculating speed of sound and attenuation coefficients. Once very precise CT data is obtained, a numerical study similar to *(Pichardo et al., 2011)* will be executed to establish these coefficients for both skull samples. These coefficients will then be used to study numerically the acoustic propagation near the skull to avoid collateral damage due to heating. An algorithm for re-focusing across the pediatric skull based on the age range will finally be designed and validated on *in-vitro* phantoms.

7. Communications:

Oral presentation:

E. Constanciel Colas, A.C. Waspe, C. Mougenot, T. Looi, S. Pichardo, J.M. Drake, *Non-invasive treatment of pediatric neurological disorders using Magnetic Resonance-guided Focused Ultrasound: Acoustic characterization of a neonate skull using a clinical HIFU system,* 27th International Symposium on Paediatric Surgical Research, Toronto, September 22nd – 23rd, 2014.

Poster:

E. Constanciel Colas, A.C. Waspe, C. Mougenot, T. Looi, S. Pichardo, J.M. Drake, *Acoustic characterization of a neonate skull using a clinical MR-Guided High Intensity Focused Ultrasound System for pediatric neurological disorder treatment planning*, 4th International Symposium Current and Future Applications of Focused Ultrasound, Washington, October 12th–16th, 2014.

8. References:

Fry, F. J., and J. E. Barger. "Acoustical properties of the human skull." *The Journal of the Acoustical Society of America* 63.5 (1978): 1576-1590.

Pichardo, S., V. W. Sin, and K. Hynynen. "Multi-frequency characterization of the speed of sound and attenuation coefficient for longitudinal transmission of freshly excised human skulls." *Physics in medicine and biology* 56.1 (2011): 219.

Wydra, A., and R. Gr Maev. "A novel composite material specifically developed for ultrasound bone phantoms: cortical, trabecular and skull." *Physics in medicine and biology* 58.22 (2013): N303.

Zaporzan, B, et al. "MatMRI and MatHIFU: software toolboxes for real-time monitoring and control of MR-guided HIFU." *Journal of Therapeutic Ultrasound* 1.1 (2013): 1-12.